

## Investigation of the phase transition in lead fluoride by proton channeling

R. E. Benenson, W. L. Roth, and W. M. Gibson

*Department of Physics, State University of New York at Albany, Albany, New York 12222*

B. Daudin and M. Dubus

*Departement de Recherche Fondamentale de Grenoble, Service des Basses Temperatures, Centre d'Etudes Nucleaires de Grenoble, Boite Postale 85 X, 38041 Grenoble CEDEX, France*

Christopher C. Jones

*Department of Physics, Union College, Schenectady, New York 12308*

H. J. Guggenheim\*

*AT&T Bell Laboratories, Murray Hill, New Jersey 07974*

(Received 19 October 1990; revised manuscript received 18 March 1991)

Axial-channeling measurements as a function of temperature have been carried out on single crystals of lead fluoride,  $\text{PbF}_2$ . The original stimulus came from the term sublattice melting, and with it the expectation that channeling by fluorine would disappear at appreciably lower temperatures than for Pb. Angular scans centered around, respectively, the  $\langle 100 \rangle$ ,  $\langle 110 \rangle$ , and  $\langle 111 \rangle$  axes were measured for temperatures ranging from 280 to 800 K. A multistring continuum model was developed in an effort to simulate the data, including the effect of displaced fluorine atoms, and, based on the model, the data indicate that the displaced fluorine atoms are neither uniformly distributed nor on octahedral sites. At 800 K, a sharp fluorine channeling minimum disappears first along the  $\langle 100 \rangle$  axis, but the measurements do not support the melting concept. The effect of the incident beam on the measurements is considered.

### I. INTRODUCTION

Superionic conductors are solids with anomalously large ionic conductivities equal to good liquid electrolytes. Phase transitions in these materials can be classified in two categories: (1) first order, typified by the 417-K transition in  $\text{AgI}$ , at which there is a discontinuity in the ionic conductivity and a change in lattice symmetry and (2) second order, typified by  $\beta\text{-PbF}_2$ , in which there is a continuous change of conductivity over a broad range of temperatures  $T \approx 475$  to 775 K, and the structure undergoes an order-disorder transition. The high conductivity of  $\text{PbF}_2$  was reported by Faraday in 1839, and for a wide range of temperatures below the melting point  $T_m$  it has the highest of any superionic conductor. Boyce and Huberman<sup>1</sup> and Chadwick<sup>2</sup> review the properties of these materials. Despite extensive experimental and theoretical studies, the structure in the high-conductivity temperature range and the conduction mechanism are still controversial. The latter is difficult to explain by thermally activated hopping of  $\text{F}^-$  ions between well-defined lattice sites, the usual mechanism of ion transport in crystals.

The transition in  $\beta\text{-PbF}_2$  is marked by a broad specific heat anomaly<sup>3</sup> centered at  $T_c = 712$  K. Below the transition,  $\beta\text{-PbF}_2$  has the fluorite structure and is almost an insulator, but above the transition it has a disordered structure in which the ionic current is carried by  $\text{F}^-$  ions which diffuse rapidly through the interstices of the cation sublattice. Several hundred degrees below  $T_c$  the con-

ductivity begins to rise with  $T$ . The activation energy  $E_{\text{act}}$  remains at about 1 eV, but then near 800 K  $E_{\text{act}}$  decreases to a few tenths eV, and the conductivity  $\sigma_c$  reaches  $400 \Omega^{-1}\text{cm}^{-1}$  and remains constant to  $T_m$  at 1178 K.<sup>4</sup>

The concept of sublattice melting has been used to describe the change at the order-disorder transition,<sup>5-7</sup> in which ions on one sublattice (F) becomes mobile within the nearly rigid framework of the other (Pb), and have liquidlike properties. A quasiliquid sublattice model would be consistent with the highly conductive state: at  $T_c$  there is no detectable change in the residual lattice crystal symmetry, negligible change in  $\sigma_c$  as  $T$  approaches  $T_m$ , a large increase in entropy at  $T_c$ , and a compensating decrease in the entropy of melting. However, the relaxation and residence times obtained with pulsed-field gradient NMR (Refs. 8 and 9) and incoherent quasielastic neutron scattering studies<sup>10</sup> support a hopping model. The anomalously high  $\sigma_c$  is explained by the creation of a large number of defect clusters.<sup>11</sup>

The sublattice melting concept is particularly applicable<sup>12</sup> to  $\text{PbF}_2$ . Its relatively simple structure suggested<sup>13</sup> that proton channeling measurements could track the increasing Pb and F thermal vibrations normal to particular crystal axes using Rutherford backscattering (RBS) and nuclear reaction analysis (NRA) simultaneously. Axial channeling measurements make use of the fact that a beam of incident charged particles entering a crystal can be steered by rows (also called strings) of its constituent atomic nuclei, provided that the beam makes a small an-

gle with a crystal axis. Evidence, at some temperature, of steering by Pb rows but not by the F anions would support the model of a fluorine liquid within a Pb lattice.

There are two ways of describing the normal (low-temperature) sites of  $\text{PbF}_2$  in its  $\beta$  phase: (1) as a simple cubic F structure centered within and having half the lattice constant of the fcc Pb structure (5.92732 Å), or (2) as a simple cubic array of F anions with Pb occupying alternate cube centers. The normal F sites are also described as tetragonal, and the empty F-cube centers as octahedral. We use description (1) when comparing channeling results with simulations below, whereas description (2) is preferable for a conduction path of displaced F anions migrating through the empty F cubes.<sup>14</sup>

Dickens *et al.*<sup>15</sup> conclude that at 800 K 30–40 % of the F anions have left their normal sites; eight possible redistributions are listed, of which three are preferred. A molecular dynamics calculation favors anion motion in the  $\langle 100 \rangle$  direction, and describes the displaced temperature-dependent F-anion concentrations as having roughly two-dimensional Gaussian shapes centered at the normal sites.<sup>16</sup> Refinements of x-ray- and neutron-diffraction data locate the displaced F anions on the  $\langle 111 \rangle$  axis.<sup>17–20</sup>

An analysis of EXAFS data suggests substantial displacements of F anions along the  $\langle 111 \rangle$  axis even at room temperature.<sup>21</sup> An article invoking light-scattering data<sup>22</sup> finds diffusion solely of  $\text{F}^-$  ions at high  $T$  inadequate to explain the data.

Channeling measurements on  $\text{UO}_2$  and  $\text{ZrO}_2$ , two other crystals having the fluorite structure, have been discussed in detail by, respectively, Eriksson and Davies<sup>23</sup> and by M. Berti *et al.*,<sup>24</sup> the analyses applied Barrett's phenomenological rules for single strings<sup>25</sup> to the diatomic case. Recently da Silva *et al.*<sup>26</sup> have reported channeling measurements on  $\text{PbF}_2$  at room temperature and at approximately 700 K using 2.52-MeV  $\alpha$  particles for both RBS and NRA.

Lead fluoride crystallizes in two forms,  $\alpha$ - $\text{PbF}_2$  with the orthorhombic  $\text{PbCl}_2$  structure and  $\beta$ - $\text{PbF}_2$  with the cubic fluorite structure. The latter form is stable from about 573 K to the melting point, and in the absence of pressure will be retained on cooling to room temperature. Throughout, the  $\text{PbF}_2$  will be assumed to have remained in its  $\beta$  phase.

Axial-channeling measurement techniques were used in the present work both to investigate the temperature dependence of the Pb and F ionic thermal vibration amplitudes transverse to the  $\langle 100 \rangle$ ,  $\langle 110 \rangle$ , and  $\langle 111 \rangle$  axes, and to test various models for the lattice location of F anions detached from their normal sites. The data were recorded as angular scans, which are a measure of the relative number of close-encounter events (collisions or near collisions) between incident protons and the  $\text{PbF}_2$  nuclei of the crystal as its axis was rotated with respect to the beam direction, taken as  $0^\circ$ . Since the incident particles were steered away from the atomic rows most strongly at  $0^\circ$ , at this angle the count rate in a detector sensitive to close-encounter events was at a minimum. As the so-called tilt angle between axis and beam was increased, the count rate increased sharply, until finally it flattened out

at a random level, as if the crystal were amorphous. Alternatively, a typical angular scan could be viewed as a sharp dip in count rate between the flat random levels at positive and negative angles. The ratio of minimum to random count rates is called  $\chi_{\min}$ , and the width of the dip  $2\psi_{1/2}$  is the difference in the tilt angles measured on both sides of  $0^\circ$  at the average of the same two count rates. Both  $\chi_{\min}$  and  $2\psi_{1/2}$  give information about the degree of atomic order in the crystal, and the width  $2\psi_{1/2}$  is sensitive to thermal vibration amplitudes; the width decreases as  $T$  increases. Typically, measurements sample the region extending to roughly 1000 Å below the crystal surface. Flux peaking, another property of channeling, is the bunching of the incident particles in regions of the channel and very useful for identifying interstitial atoms, here, displaced F.

## II. EXPERIMENTAL METHODS

We have measured the channeling angular distributions centered around the  $\langle 100 \rangle$ ,  $\langle 110 \rangle$ , and  $\langle 111 \rangle$  axes for Pb and F simultaneously over a range  $280 < T < 800$  K. The method closely followed that of Hellborg,<sup>27,28</sup> who investigated several other fluorides. At proton energies just above the 876-keV  $^{19}\text{F}(p,\alpha)^{16}\text{O}$  resonance, RBS and  $^{16}\text{O}$   $\gamma$  rays identified, respectively, close-encounter events involving Pb or F. After mounting the crystal in the goniometer and locating one of the axes from its RBS  $\chi_{\min}$ , the count rate as a function of angle was recorded on either side of  $0^\circ$  until both random levels were identified.

A  $\text{PbF}_2$  single-crystal ingot approximately 6 cm long by 1.5 cm wide by 1 cm thick was grown at AT&T Bell Laboratories.<sup>29</sup> The best surfaces for channeling were obtained by conchoidal fracture, and selected fragments showed unusually low  $\chi_{\min}$  for this compound at room temperature (occasionally less than 0.05). Commercial crystals typically had  $\chi_{\min}$  greater than 0.3.

The major part of the present axial channeling measurements were performed at the SUNY/Albany 4 MV Dynamitron accelerator laboratory (SUNYA). Subsequently,  $\langle 100 \rangle$  and  $\langle 111 \rangle$  angular scans were remeasured at the Centre d'Etudes Nucleaires de Grenoble (CENG) 2.5 MV van de Graaff accelerator, again using fragments from the same AT&T ingot.

After being heated to over 770 K and allowed to cool, a previously clear crystal almost always was covered by a gray surface layer, and then showed very poor channeling characteristics. This layer has been attributed to either an oxide,<sup>14</sup> or to dissociation.<sup>22</sup>  $\text{PbF}_2$  appears to be quite reactive at elevated temperatures; copper was much superior to stainless steel as a crystal holder material. Build-up of the layer was slowed by surrounding the entire rotatable crystal holder assembly with a cylinder held at liquid  $\text{N}_2$  temperature. In the one case that the crystal could be temperature recycled, channeling suddenly disappeared just before 770 K was reached again. The dependence of the thick-target yield of  $^{19}\text{F}(p,\alpha)^{16}\text{O}$   $\gamma$  rays on proton energy  $E_p$  from fresh and discolored crystals showed no difference, suggesting that the surface lay-

er was not disassociated Pb. Each new fragment for another SUNYA run was oriented by identifying planar intersections.

When tilt angle  $\theta$  scans showed appreciable planar effects, the scans were then changed to either a combination of tilt and azimuthal angle  $\varphi$ , or just  $\varphi$ , and the equivalent  $\theta$  calculated.

The experimental arrangement used at SUNYA is shown schematically in Fig. 1. The angular divergence of the 1-mm diam. proton beam was limited to less than  $0.02^\circ$  by means of collimators. The target chamber was actually a Dependex tee section with its long dimension vertical; the goniometer with the heated target holder fitted into the upper opening of the tee, and a coaxial liquid  $N_2$  can mounted on an external cold finger fitted into the lower opening. The 885–890-keV proton beam first passed through an annular ring containing the slightly off-axis RBS solid-state detector protected from target heat by a  $1\text{-}\mu\text{m}$ -thick Ni foil. An external 12.5-cm long by 12.5-cm diam. NaI detector butted against the vertical section of the tee to record the  $\gamma$  rays with energies

greater than 3 MeV from the  $^{19}\text{F}(p,\alpha)^{16}\text{O}$  reaction.

The crystal fragments were irregular in shape, with lateral (surface) dimensions ranging from roughly 5 to 7 mm, and with a variable thickness ranging up to several mm. The all-copper crystal holder consisted of a box lined with soft foil which pressed the crystal against the box cover. The cover had a rectangular aperture to admit the beam. The heater was directly behind, and in contact with, the holder. The chromel-alumel thermocouple junction was caught under one of the screws which held the cover to the box (away from the heater) and was considered to be at the crystal temperature  $T$  to within a fraction of a degree. However, at the higher temperatures  $T$  drifted during a scan by as much as  $\pm 5$  K.

The heater connections interfered with beam current integration, so that measurements above room temperature were taken using timed runs of a steady beam current, typically 0.3 nA. Current integration was used for all room-temperature angular scans from which a fixed run time per data point of a scan at elevated temper-

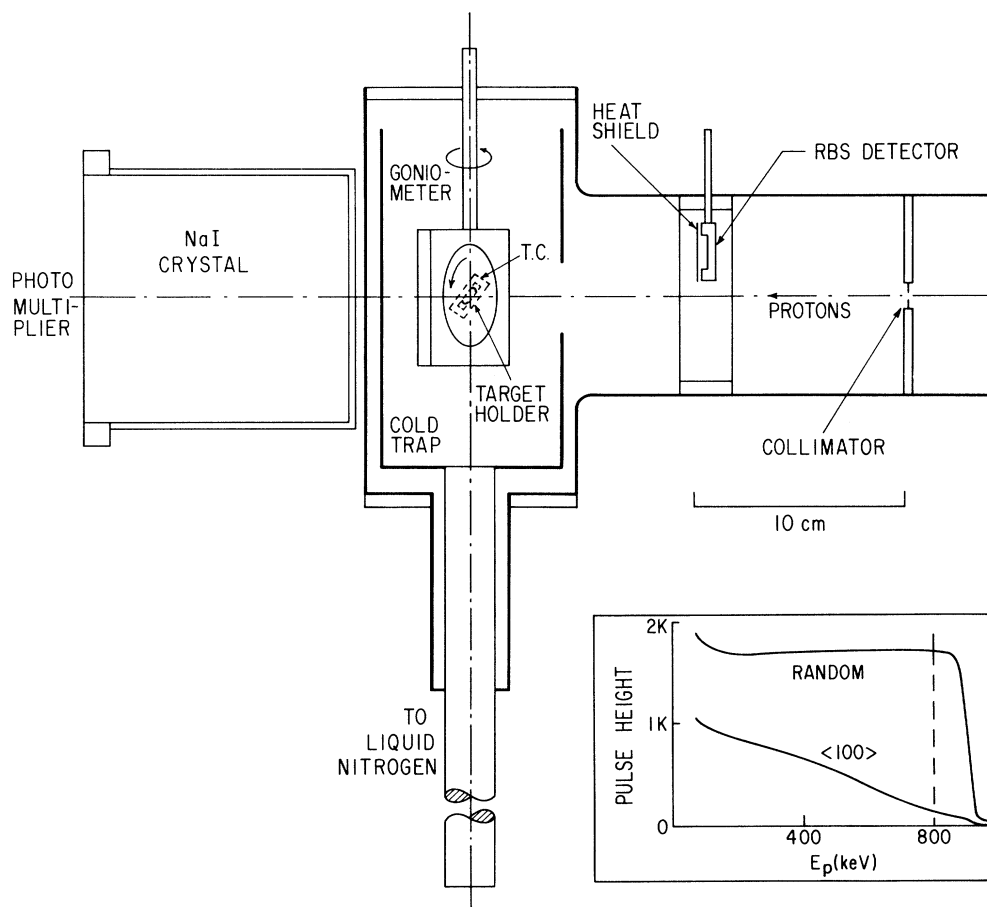


FIG. 1. Schematic section view of the SUNY experimental arrangement. The portion of the goniometer assembly which holds the crystal is shown as having its axis rotated away from the beam direction, and T.C. represents the thermocouple junction attached to the crystal holder. A thin Ni foil protects the RBS detector from infrared radiation. Inset: random and  $\langle 100 \rangle$  aligned pulse height distributions from the RBS detector. The vertical dashed line represents the minimum level for a detector pulse to be recorded.

atures was chosen to be in the range of 20 to 30 s, corresponding to integrated proton charges of 6 to 9 nC. By means of a DPDT switch the heater could be disconnected for a short period, and the stability of the beam

checked. Most  $\langle 100 \rangle$  and  $\langle 110 \rangle$  angular scans were remeasured in separate runs.

The inset in Fig. 1 shows two spectra from the RBS detector taken at room temperature for the proton beam

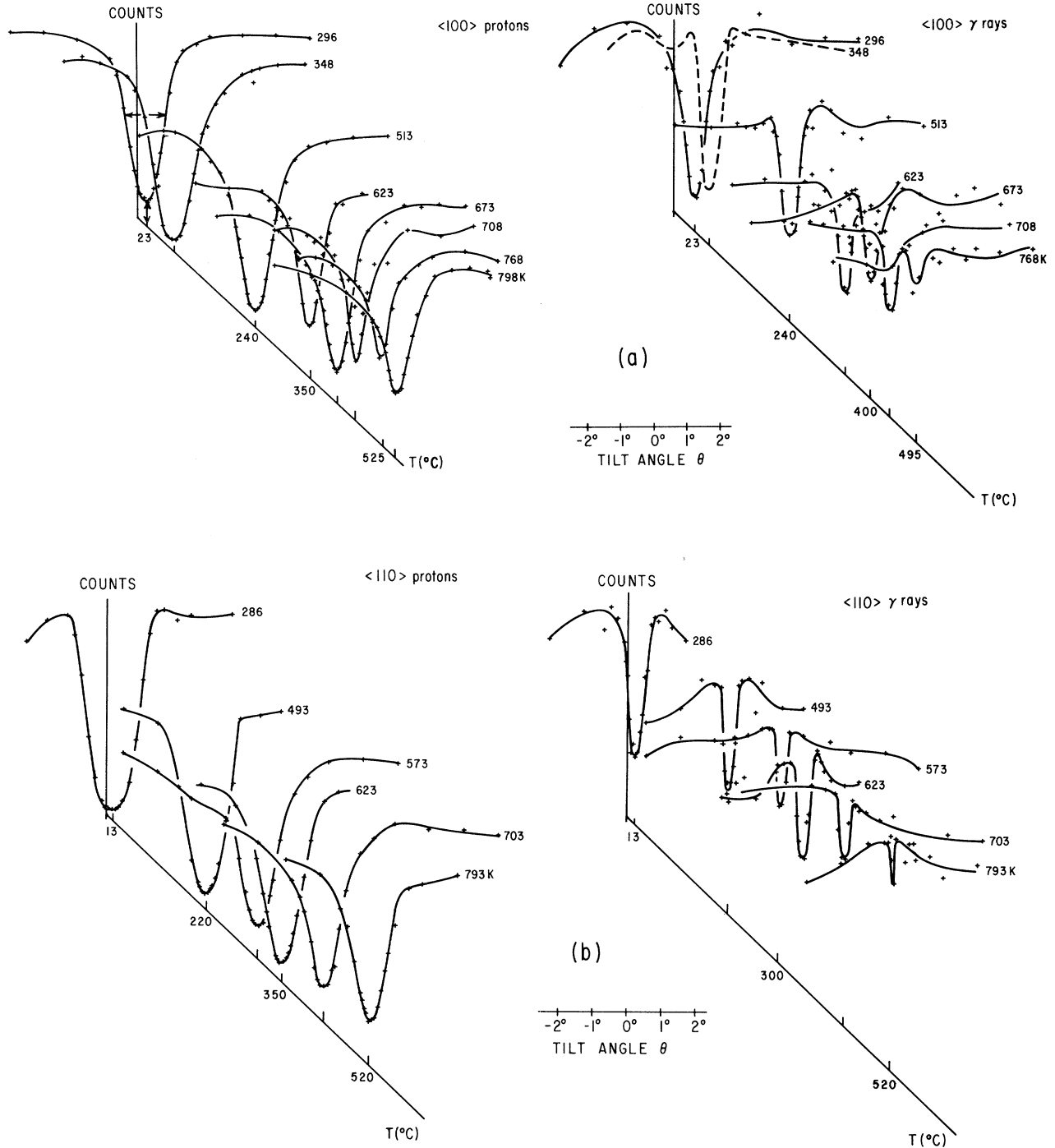


FIG. 2. (a) Experimental angular scans for  $\langle 100 \rangle$  axial channeling by Pb (left diagram) and F (right diagram) as isometric plots of, respectively, proton and  $\gamma$ -ray count rates vs tilt angle. The individual scans are labeled by temperature K, with respective origins labeled by  $T$  ( $^\circ\text{C}$ ). Count rates are normalized to the random level. Some scans which are not shown appear in Fig. 3. The solid lines are a guide to the eye. The horizontal and vertical arrows on the 296-K proton scan show, respectively, how  $2\psi_{1/2}$  and  $\chi_{\min}$  are measured. (b) Experimental angular scans for  $\langle 110 \rangle$  axial channeling. Otherwise, as in (a). (c) Experimental angular scans for  $\langle 111 \rangle$  axial channeling. Otherwise, as in (a).

in the random direction and aligned with the  $\langle 100 \rangle$  axis. The vertical dashed line indicates, approximately, the level above which pulses were accepted as counts (to assure near-surface backscattering), so that  $\chi_{\min}$  is simply the ratio of aligned to random counts in the two spectra, here for  $\langle 100 \rangle$ .

Partial angular scans at  $E_p \approx 850$  keV, below the 876-keV resonance energy, allowed subtracting contributions from lower energy resonances excited deeper within the crystal.

At the CENG, a computer-controlled goniometer at the center of a scattering chamber contained the heated sample holder, and a rotating vane sampled the beam. The crystals were cut, polished, and their axes identified by x rays, before being mounted in the goniometer. The chamber was cryopumped to a vacuum of better than  $10^{-7}$  torr; no additional liquid  $N_2$  trapping was provided.

### III. EXPERIMENTAL RESULTS

The SUNY angular scans for Pb (proton counts) and F ( $\gamma$ -ray counts) are represented by isometric plots spaced along a  $T$  ( $^{\circ}C$ ) axis on Figs. 2(a), 2(b), and 2(c), corresponding, respectively, to  $\langle 100 \rangle$ ,  $\langle 110 \rangle$ , and  $\langle 111 \rangle$  axial channeling. Not all scans have been included. These plots are normalized to their respective random levels.

As expected, the  $\langle 100 \rangle$  and  $\langle 110 \rangle$  scans are narrower and shallower for F than for Pb, but in the mixed-string  $\langle 111 \rangle$  direction they are quite similar, which also shows that the effective sampling depth was almost equal for Pb and F.

The vertical and horizontal arrows on the 297-K proton scan of Fig. 2(a) illustrate, respectively, the terms  $\chi_{\min}$  and  $2\psi_{1/2}$  which characterize an angular scan;  $\chi_{\min}$  is the count rate minimum at  $0^{\circ}$ . Calling the random-level count rate at large tilt angles  $R$ , then  $2\psi_{1/2}$ , assuming symmetry around  $0^{\circ}$ , is the difference between tilt angles  $\theta$  on either side of  $0^{\circ}$  for which the count rate is  $\frac{1}{2}(R + \chi_{\min})$ .

The highest temperature  $\langle 100 \rangle$ ,  $\langle 111 \rangle$ , and  $\langle 100 \rangle$  scans are expanded in Fig. 3, including those omitted for clarity in Fig. 2. Error bars are based on counting statistics only. The  $\langle 100 \rangle$  channeling dip disappears in going from 768 to 798 K as seen in the upper two scans in Fig. 3. (The highest  $T$  for the  $\langle 100 \rangle$  data was actually  $798 \pm 5$  K, rather than 773 K reported earlier.<sup>30</sup>) The lower left plot shows that steering by  $\langle 111 \rangle$  strings is strong at 768 K. Weak channeling is still present when viewed along  $\langle 110 \rangle$  at 793 K. The light solid curves drawn on Fig. 3 represent the simultaneous Pb scans, somewhat asymmetric due to planar effects. Since the Pb and F  $\langle 111 \rangle$  scans essentially coincided, the Pb curve was omitted on

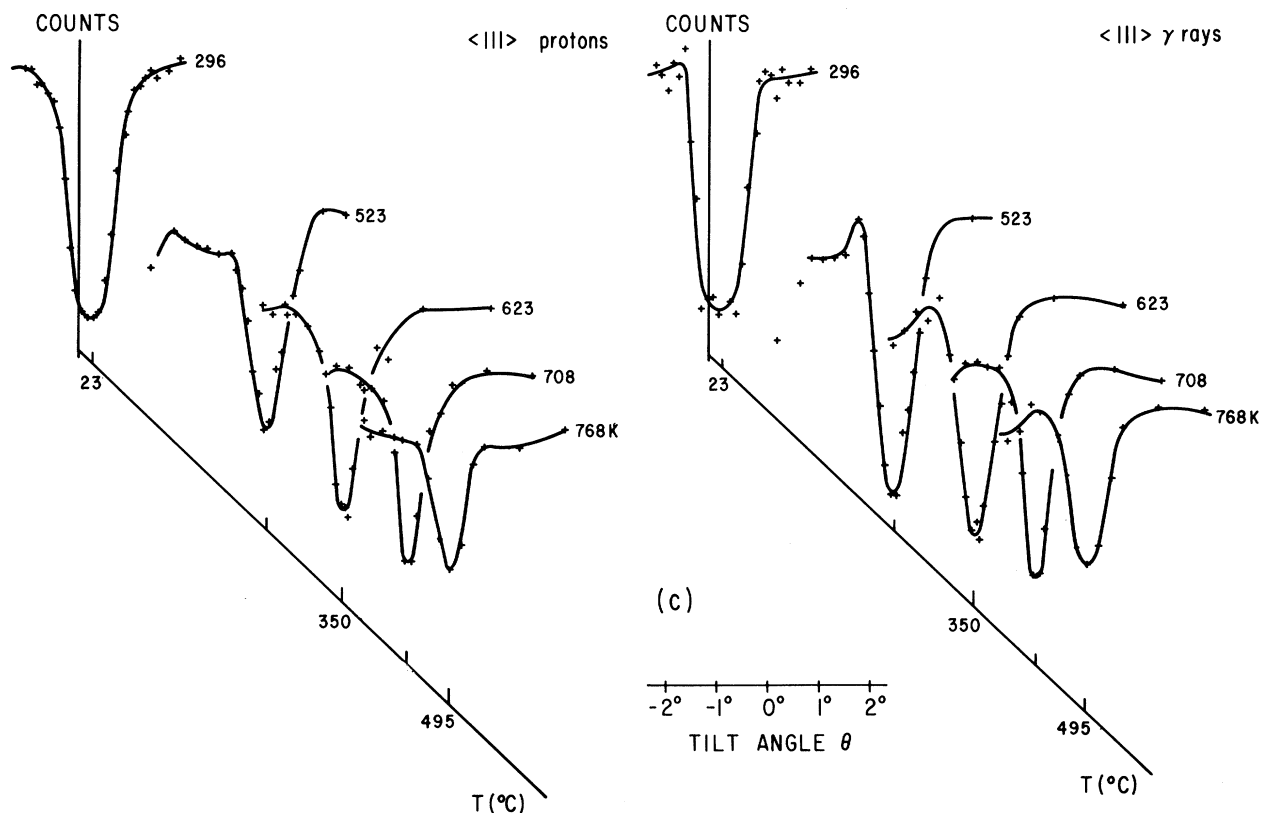


FIG. 2. (Continued).

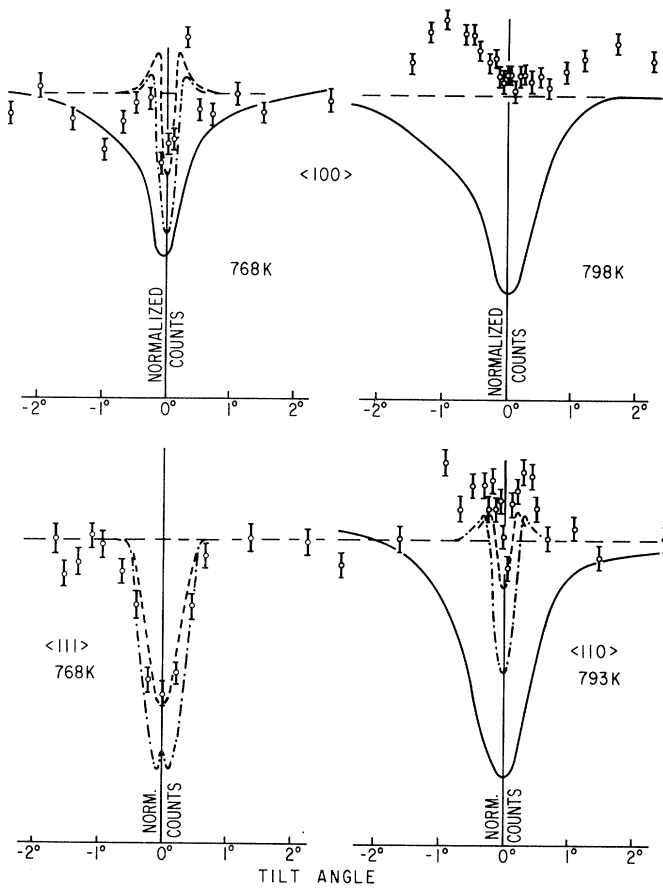


FIG. 3. Expanded plots of the angular scans near the high temperature limit of the data. The error bars are drawn through F data points, and the curves below represent the Pb data taken simultaneously. No Pb curve is shown for  $\langle 111 \rangle$  since it essentially runs through the F data points [see Fig. 2(c)]. The dot-dash and dashed curves are from model calculations for, respectively, the fraction of F ions remaining on a string  $f = \frac{2}{3}$  and  $f = \frac{1}{3}$ . The off-string F is assumed to have a Gaussian distribution. The small peak at the center of the  $\langle 111 \rangle$  simulation is discussed in the text.

this plot to avoid confusion. The broken curves are from model calculations discussed below.

The CENG scans were made with better charge integration and more reliable random levels than at SUNY, but the  $\chi_{\min}$  were higher, possibly due to the slightly larger  $E_p = 900$  keV, or different surface preparation, and planar effects were more pronounced. At 700 K,  $\langle 110 \rangle$  evidence for F structure was still present, and again Pb and F  $\langle 111 \rangle$  scans were very similar throughout the T range.

The temperature dependence of the widths  $2\psi_{1/2}$  are shown in Fig. 4 for each of the three axes. Widths of most SUNY scans were obtained from a least-squares polynomial fit to data points corresponding to each side and minimum. When scans were asymmetrical due to planar effects,  $2\psi_{1/2}$  was then taken as twice the smaller of the

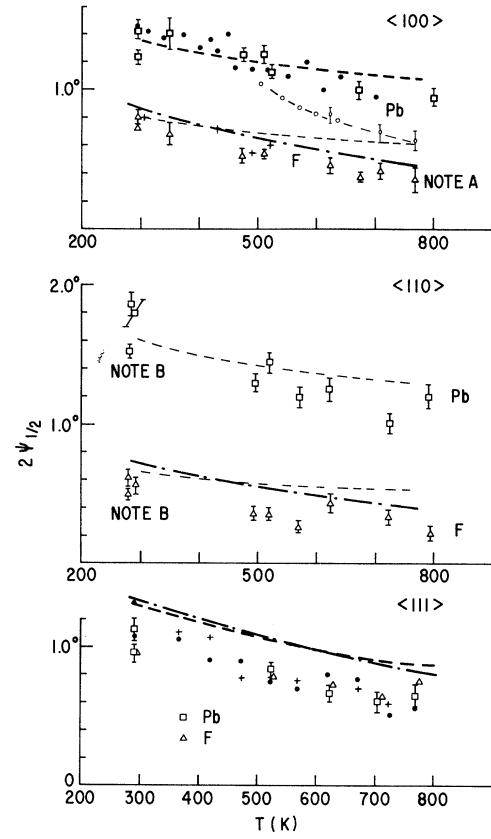


FIG. 4. The temperature dependence of the widths  $2\psi_{1/2}$  for the three axes. The squares and triangle are SUNY results, respectively, for Pb and F. The filled circles and crosses are corresponding CENG results. The light open diamonds and circles are the second Pb  $\langle 100 \rangle$  branch discussed in the text. Dashed line: values calculated from single-string theory. Dot-dash line: values calculated from the multistring model discussed in the text. Note A: The F channeling dip disappeared just above this temperature. Note B: The lowest points were after recycling back from the highest T.

two half-widths. For the CENG data, reliable  $2\psi_{1/2}$  values could be obtained by extending the lower part of the dip up to the random level. Uncertainties in the choice of random levels, the shape of the dip at the sides, and exact position of each minimum all entered into the error bars in Fig. 4. The SUNY and CENG values are shown, respectively, for Pb as squares and filled circles, and for F as triangles and crosses, and in general agree well.

Mean-square thermal vibration amplitudes  $\langle u^2 \rangle$  needed in single- and multi-string model calculations, as well as the Debye temperatures of 129 K for Pb and 332 K for F, were based on Debye-Waller factors B given by Dickens *et al.*<sup>15</sup>

Values of  $2\psi_{1/2}$  calculated from single-string theory<sup>25,31</sup> are shown on Fig. 4 as dashed lines; for the  $\langle 111 \rangle$  mixed string, the Pb and F parameters were weighted 1:2 and,

as suggested,<sup>24</sup> using the larger (F) thermal vibration amplitudes.

An unresolved problem with the Pb  $\langle 100 \rangle$  angular scans is that above 600 K a second, and lower set of  $2\psi_{1/2}$  values (with higher  $\chi_{\min}$ ) appear in both the SUNY and CENG data. These are shown, respectively, in the Fig. 4 upper plot as open diamonds and circles. The corresponding scans in Fig. 2(a) are at 623, 708, and 768 K, the latter also in Fig. 3. The upper branch agrees much better with single-string model calculations. We believe that the lower set of values obtained during heating (SUNY) or cooling (CENG), were due to either a shift of the crystal in its holder or stress-induced mosaic spread, but the double occurrence of two sets is worth noting. Widths for F  $\langle 100 \rangle$  do not show the split.

Experimental  $\chi_{\min}$  versus  $T$  are shown in Fig. 5. In general, experimental  $\chi_{\min}$  are larger than predicted by calculations, as discussed below. Only the lowest  $\chi_{\min}$  achieved for a given set of experimental conditions are plotted. While the individual values shown would have most a few percent uncertainty, there were considerable variations between crystal fragments. For the single-string model, calculated  $\chi_{\min} = 3 \text{ Nd} \langle u_2^2 \rangle$ , where Nd are the atoms/cm<sup>2</sup> viewed along a given axis and  $\langle u_2^2 \rangle$  are the transverse thermal vibration amplitudes,<sup>25</sup> and were typically  $\frac{1}{2}$  those shown in Fig. 5 for Pb, and  $\frac{1}{3} - \frac{1}{5}$  those shown for F.

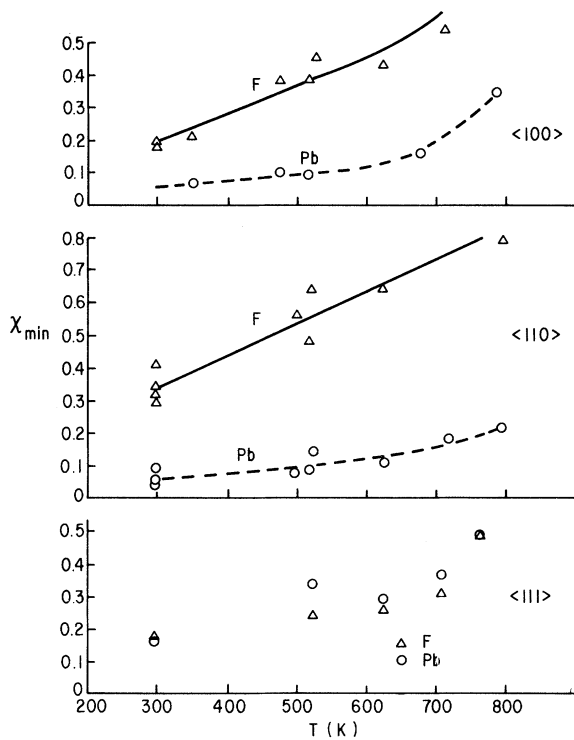


FIG. 5. Experimental  $\chi_{\min}$  vs  $T$  for the three axes. The values plotted are the lowest for runs made under similar conditions, since many factors usually tend to raise experimental  $\chi_{\min}$  above calculated values.

#### IV. COMPUTER SIMULATION

In an attempt to interpret the influence of displaced F anions on the channeling data, theoretical angular scans for F were generated by summing thermally spread string potentials, as described in the preliminary report,<sup>30</sup> but now with (1) a more correct choice of  $\langle 100 \rangle$  and  $\langle 110 \rangle$  strings, (2) extending the calculations to the  $\langle 111 \rangle$  axis, and (3) including the effects of displaced F atoms. (Simulations using thermally spread string potentials based on anharmonic vibrations<sup>1</sup> were not attempted.) Model calculations of channeling by diatomic compounds are seldom found in the literature, although a paper on GaAs has recently appeared<sup>32</sup> and Ref. 26 data will likely be compared with a similar Monte Carlo approach.

The end result of the present simulation is  $P_c(\theta)$ , the collision probability versus tilt angle. In brief, thermally spread string potentials were calculated according to the method of Appleton *et al.*<sup>33</sup> using the Lindhard potential.<sup>34</sup> Next, the multistring potential  $U(x,y)$  for the (100) plane was taken as the sum of contributions from nine Pb and four F strings inside and bounding a lattice cell, and 8 Pb and 12 F strings outside; the corresponding numbers for (110) are 8 Pb and 6 F, to which were added 10 Pb and 10 F strings outside. The (111) potential was established with a string at the center of a hexagonal arrangement surrounded, in turn, by 12 strings, 19 in all. Equipotential contours surrounding the Pb or F strings which penetrate, respectively, the (100) or (110) planes through the upper right quadrant of a cell are shown in Fig. 6. [The (111) contours are nearly circles which surround the identical strings.] These multistring  $U(x,y)$  determined the flux integral  $F(x,y,\theta)$  needed to evaluate  $P_c$ . Integrations were performed by summing over, for reasons of symmetry, 5000 squares of a triangle in the (100) projection, half of a quadrant; 10 000 (110) quadrant rectangles; and 5000 (111) rectangles making up a triangle which was  $\frac{1}{12}$  of a hexagon. (Flux peaking, mentioned in the Introduction, occurs in regions of lowest potential; for example, between the strings of Fig. 6.) Assuming statistical equilibrium<sup>35</sup> for an estimated 1200-Å depth,

$$F(x,y,\theta) = \int_{E_T \geq U(x,y)} \frac{dx_{\text{in}} dy_{\text{in}}}{A(E_T)}. \quad (1)$$

An incoming projectile which enters the differential area  $dx_{\text{in}} dy_{\text{in}}$  with transverse energy  $E_T > U(x_{\text{in}}, y_{\text{in}}) + E_p \theta^2$  is assumed capable of reaching any point in the accessible area  $A(E_T)$ , such that  $E_T \geq U(x,y)$ . In the actual calculation,  $F(x,y,\theta)$  was stored as  $F(U(x,y),\theta)$  in one-volt intervals of  $U$ . As a given potential interval was encountered, another grid square was added to the area sum corresponding to the interval index.

Finally,

$$P_c = \int \sum_{i \text{ strings}} \exp \left[ \frac{-r_i^2}{\sigma^2} \right] F(x,y,\theta) dx dy, \quad (2)$$

transformed into

$$P_c = \sum_{x,y} \sum_{i \text{ strings}} \exp \left[ \frac{-r_i^2}{\sigma^2} \right] F(U(x,y),\theta) \Delta x \Delta y, \quad (2a)$$

where  $r_i^2 = x_1^2 + y_1^2$  is measured from a given F string, and

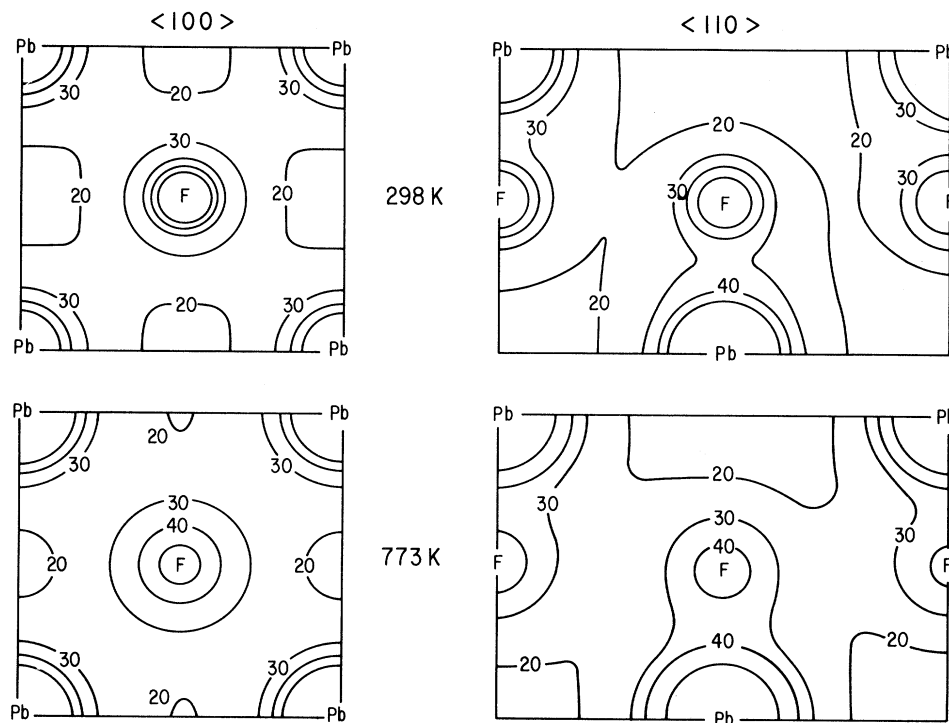


FIG. 6. Equipotential contours in the upper right quadrant of lattice cell projections in the (100) and (110) planes obtained with the multistring model described in the text. The positions of the Pb and F strings are labeled accordingly. Successive contours inward toward a string are in 10-V intervals. The potentials between the 20-V contours exceed 10 V, and are quite flat.

$\sigma^2 = \frac{2}{3} \langle u^2 \rangle$ .  $P_c$  was calculated only for F.

The values of  $2\psi_{1/2}$  as a function of  $T$  with all F assumed vibrating around normal sites are shown as dot-dash lines on Fig. 4, and are in slightly better agreement with the data than in Ref. 30; however,  $\chi_{\min}$  remain  $\frac{1}{3}$  the experimental values shown in Fig. 5. In the absence of liberated F, the model gave pronounced channeling dips even at 873 K.

The calculation of  $P_c$  at 773 K with a fraction of F atoms serving only as scattering centers, but not providing steering, consisted of (1) introducing a factor  $f$  into each F potential to weaken the F strings, as if the average spacing is increased, and (2) confining the  $(1-f)$  liberated atoms to selected lattice positions. Contributions to  $P_c$  were calculated as areas in the plane weighted  $f:1-f$  according to whether or not the ions or atoms remained on a string. Dickens *et al.*<sup>15</sup> indicate  $f \approx \frac{2}{3}$  at 773 K, and simulations were limited to this value and  $f = \frac{1}{3}$ . To approximate various proposed F arrangements at ionic conductivity temperatures, the atoms were placed, (A) with two-dimensional Gaussian distributions of varying widths centered around the normal sites<sup>16</sup> or (B) uniformly distributed (model III of Ref. 15, also in effect the excluded-volume model,<sup>1</sup> since the proton flux is minimal at the Pb sites); or (C) at the octahedral sites;<sup>1</sup> and, finally, (D) in strips (i) along the diagonal of Fig. 5 (the projection of the  $\langle 111 \rangle$  axis<sup>17-20</sup>), (ii) along the outer edges, and (iii) in re-

gions of high particle flux. At high  $T$  shapes were much more sensitive to  $f$  than to  $\langle u^2 \rangle$ . Once files were created for a potential field and for the corresponding flux distribution, angular scans according to displaced-F arrangements could be calculated quickly. All the simulations were carried out on a desktop computer. The model calculations do not rule out F anions becoming distributed along  $\langle 111 \rangle$ , because potentials based on F strings no longer apply. The simulations did not generate the broad rise surrounding the dip in the actual  $\langle 110 \rangle$  scans, also seen in Ref. 26, but this may be a planar effect.

Calculations based on assumption (A) are compared with the data in Fig. 3, since this assumption gives the best overall consistency with the experimental results. The Gaussian standard deviations in this model are between 1 and 1.5 Å. The dot-dash curves are for  $f = \frac{2}{3}$  and the dashed curves for  $f = \frac{1}{3}$ . The small rise at the center of the  $\langle 111 \rangle$  simulation in Fig. 3 is the result of flux peaking; for a smaller standard deviation it would vanish. Choice (D i), diagonal strips, raised  $\chi_{\min}$  satisfactorily for  $\langle 110 \rangle$ , relative to (A) or (B), but lowered it for  $\langle 100 \rangle$ , as shown in Fig. 7(a). The effect of assumption (C), displaced F in octahedral sites, appears in Fig. 7(b) as the sharp  $\langle 110 \rangle$  central maximum. Assumption (B), the uniform distribution, creates the center peak of the  $\langle 111 \rangle$  scan shown in Fig. 7(c). Neither of the latter two simulations conforms to the data.

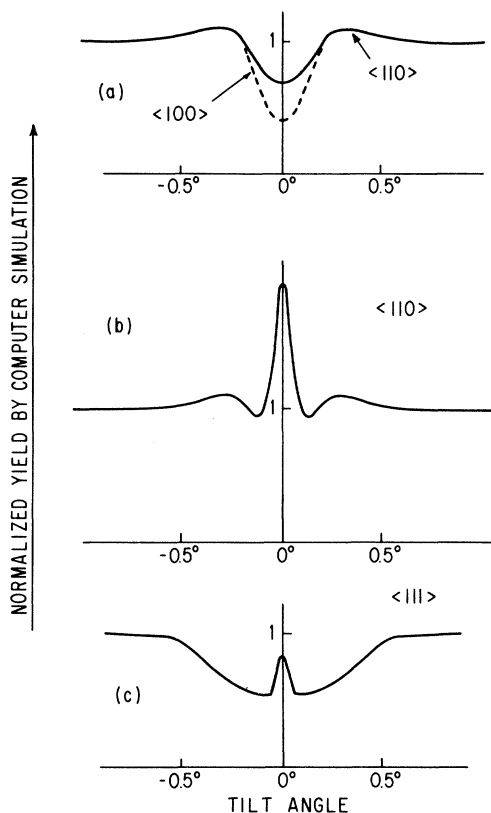


FIG. 7. (a) Simulated angular scans for  $\langle 100 \rangle$  and  $\langle 110 \rangle$  channeling at  $T = 773$  K assuming that  $\frac{1}{3}$  of the F anions are detached from their normal sites and are located in a narrow band extending along the inner half of the  $\langle 111 \rangle$  diagonal. (b) As in (a), but with the detached F anions localized near the octahedral sites between Pb strings. (c) As in (a) and (b), but assuming that the detached  $\frac{1}{3}$  of F anions are uniformly distributed throughout the lattice cell volume.

## V. DISCUSSION AND CONCLUSIONS

At temperatures well below  $T_c$  the channeling measurements show that essentially all  $\text{Pb}^{2+}$  and  $\text{F}^-$  ions are on a lattice, which supports the generally accepted view that  $\beta\text{-PbF}_2$  has the fluorite structure, and disagrees with the EXAFS study and (except for the mysterious second Pb  $\langle 100 \rangle$  branch), implications of the light-scattering measurements. The  $2\psi_{1/2}$  values for  $\langle 111 \rangle$  are in poorest agreement with model calculations, indicating larger than expected thermal vibration amplitudes. Even if F anions are displaced along this axis, steering by Pb should dominate.

Judging from Figs. 4 and 5, there are no apparent discontinuities in  $2\psi_{1/2}$  or  $\chi_{\min}$  at the 712-K specific heat anomaly. Some F-lattice structure exists, at least partially, right through the phase transition, and even the 798-K  $\langle 100 \rangle$  data in Fig. 3 appears to have some shape, although the channeling dip has disappeared. A structure which is not completely amorphous would argue against

the concept of sublattice melting.

There are strong similarities in the present proton and Ref. 26  $\alpha$ -particle data, particularly at elevated temperatures: the dip first disappears along  $\langle 100 \rangle$  (however, at 700 K see below), the  $\langle 110 \rangle$  F angular scans are similarly atypical, and there are deep and nearly identical Pb and F scans along  $\langle 111 \rangle$ , with no indication of a flux-peaking effect.

We assume that if the central peak predicted by the computer simulations for a uniform distribution of detached F anions were present in a  $\langle 111 \rangle$  angular scan, as in Fig. 7(c) some evidence would have appeared among the three sets of experiments. Consequently, the  $\langle 111 \rangle$  data rule out both a uniform distribution of liberated F anions and the excluded-volume model.<sup>1</sup> Compared to Fig. 7(b), the absence of the sharp central peak in the  $\langle 110 \rangle$  data show that these anions do not populate the octahedral sites. The most general fit to experiment along all three axes appears to be a Gaussian distribution around an F string.<sup>16</sup> The  $\chi_{\min}$  below 800 K are more consistent with about  $\frac{1}{3}$  anions remaining on the string, rather than  $\frac{2}{3}$ , but multiple scattering by other lattice ions and crystal imperfections usually cause experimental  $\chi_{\min}$  to be higher than predicted.

Many structure analyses place the displaced  $\text{F}^-$  anions along the  $\langle 111 \rangle$  axis, but disagree about the distribution. For large enough displacements from normal sites,  $\langle 100 \rangle$  and  $\langle 110 \rangle$  strings would be quite uneven, and multiple scattering is likely to destroy channeling. The present work does not permit a more definite statement.

Fluorine vacancy-interstitial pairs created by the incident beam might explain the disappearance of the  $\langle 100 \rangle$  channeling dip at 800 K with protons and at 700 K with  $\alpha$  particles,<sup>26</sup> in other words, the measurement itself might have affected the result. Nelson<sup>36</sup> notes the anisotropy of displacement energy  $E_d$ , the energy needed to form such pairs, and cites the Erginsoy *et al.*<sup>37</sup> calculations which, for iron, show  $E_d$  is least along  $\langle 100 \rangle$ . The number of vacancies created by  $\alpha$  and proton beams were calculated with TRIM<sup>38</sup> using a range of  $E_d$ ; the nominal value at room temperature is about 15 eV. Assuming  $E_d$  is closely related to the activation energy  $E_{\text{act}}$ , the latter decreases considerably very near 800 K (see Introduction). For 2.5-MeV  $\alpha$  particles, trial  $E_d$  of 10, 2, 1, and 0.5 eV, led to, respectively, 1, 6, 13, and 27 vacancies (assumed F) per incident particle. The corresponding numbers for protons were, respectively, much less than 1, less than 1, 2, and 6 vacancies per ion. For a 1-mm-diam. beam depositing, typically, of order  $25 \times 10^{12}$  protons (4  $\mu\text{C}$  of collected charge), and  $E_d = 0.5$  eV we estimate that 4% of the F present would be displaced; but if  $E_d$  became much less than 0.5 eV at 800 K, proton-liberated F could eradicate the channeling dip. Electrostatic forces exerted by the beam on F ions could also help explain the  $\alpha$ -proton temperature discrepancy.

Since the channeling dip first disappears along  $\langle 100 \rangle$ , whether  $E_{\text{act}}$  is anisotropic, or is evidence that an electric field will move  $\text{F}^-$  ions most easily along this axis argues, in our view, for superionic conduction predominantly in the  $\langle 100 \rangle$  direction.

The multistring continuum model calculations described above can easily be applied to channeling measurements on other crystals having the fluorite structure, including stabilized zirconia, uranium dioxide, and a number of hydrides (deuterated).

#### ACKNOWLEDGMENTS

We express sincere thanks to Dr. V. K. Tikku and Dr. H-S. Jin for their assistance in the early stages of the SUNY work.

\*Current address: 37 Sentinel Dr., Washington Crossing, PA 18977.

<sup>1</sup>J. B. Boyce and B. A. Huberman, *Phys. Rep.* **51**, 189 (1979).

<sup>2</sup>A. V. Chadwick, *Radiat. Eff.* **17**, 74 (1984).

<sup>3</sup>W. Shroter and J. Nolting, *J. Phys. (Paris)* **41**, C6-20 (1980).

<sup>4</sup>C. E. Derrington and M. J. O'Keeffe, *Nature (London)* **246**, 44 (1973).

<sup>5</sup>M. J. Rice, S. Strassler, and G. A. Toombs, *Phys. Rev. Lett.* **32**, 596 (1974).

<sup>6</sup>B. A. Huberman, *Phys. Rev. Lett.* **32**, 1000 (1974).

<sup>7</sup>C. E. Derrington, H. Navrotsky, and M. L. Keffe, *Solid State Commun.* **18**, 47 (1976).

<sup>8</sup>R. E. Gordon and J. H. Strange, *J. Phys. C* **11**, 3213 (1978).

<sup>9</sup>R. E. Gordon and J. H. Strange, *Faraday Symp. Chem. Soc.* **13**, 153 (1978).

<sup>10</sup>M. T. Hutchings, in *Neutron Scattering—1981*, Proceedings of the Symposium on Neutron Scattering, Argonne National Laboratory, 1981, edited by John Faber, Jr., AIP Conf. Proc. No. 89 (AIP, New York, 1982), p. 209.

<sup>11</sup>C.R.A. Catlow, J. D. Comins, F. A. Germano, R. T. Hartley, W. Hayes, and I. B. Owen, *J. Phys. C* **14**, 329 (1981).

<sup>12</sup>C.R.A. Catlow, *Comments Solid State Phys.* **9**, 157 (1980).

<sup>13</sup>R. E. Benenson, W. L. Roth, V. K. Tikku, H-S. Jin, and W. L. Gibson, in Proceedings of the Electrochemical Society Meeting, Montreal, 1982 [*J. Electrochem. Soc. Proc.* **129**, 143C (1982)].

<sup>14</sup>J. M. Oberschmidt and D. Lazarus, in *Fast Ion Transport in Solids*, edited by P. Vashishta, J. N. Mundy, and G. K. Shenoy (Elsevier-North-Holland, Amsterdam, 1979), p. 691.

<sup>15</sup>M. H. Dickens, W. Hayes, M. T. Hutchings, and C. Smith, *J. Phys. C* **15**, 4043 (1982).

<sup>16</sup>A. B. Walker, M. Dixon, and M. J. Gillan, *J. Phys. C* **15**, 4061 (1982).

<sup>17</sup>S. M. Shapiro and F. Reidinger, *Physics of Superionic Conductors*, edited by M. B. Salamon (Springer, Berlin, 1979), pp. 45-75.

<sup>18</sup>K. Koto, H. Schultz, and R. A. Huggins, *Solid State Ionics* **3,4**, 381 (1981).

<sup>19</sup>H. Schulz, E. Perenthaler, and U. H. Zucker, *Acta Crystallogr. A* **38**, 729 (1982).

<sup>20</sup>H. Schulz, *Annual Review of Materials Science* **12**, edited by R. A. Huggins, R. H. Bube, and D. A. Vermilyea (Annual

Reviews Inc., Palo Alto, CA, 1982), p. 351.

<sup>21</sup>N. Kamijo, K. Koto, Y. Ito, H. Maeda, K. Tanabe, M. Hilda, and H. Terakuchi, *J. Phys. Soc. Jpn.* **53**, 4210 (1984).

<sup>22</sup>J. Briggs, P. R. Findley, Z. L. Wu, W. C. Walker, and D. Nicoli, *Phys. Rev. Lett.* **47**, 1011 (1981).

<sup>23</sup>L. Eriksson and J. A. Davies, *Ark. Fys.* **39**, 439 (1969).

<sup>24</sup>M. Berti, A. V. Drigo, C. Cohen, J. Siejka, and M. M. Tosic, *Nucl. Instrum. Methods* **199**, 605 (1982).

<sup>25</sup>J. H. Barrett, *Phys. Rev. B* **3**, 1527 (1971).

<sup>26</sup>R. C. Da Silva, D. O. Boerma, and H. W. Den Hartog, *Nuclear Physics Applications on Materials Science*, edited by E. Recknagel and J. C. Soares (Kluwer Academic, Dordrecht, 1988), p. 393.

<sup>27</sup>R. Hellborg, *Phys. Scr.* **3**, 279 (1971).

<sup>28</sup>R. Hellborg, *Phys. Scr.* **4**, 203 (1972).

<sup>29</sup>High-purity Pb was treated with acetic acid, and the resulting lead acetate solution then reacted with 48% HF. The precipitate was slowly heated in a gas mixture consisting of HF vapor and N<sub>2</sub> in the ratio 1:9. Following this, the powder which resulted was heated in a pyrolytic graphite boat, and ingots were then made by horizontal zone melting in the same gas mixture.

<sup>30</sup>R. E. Benenson, *Nucl. Instrum. Methods* **B45**, 499 (1990).

<sup>31</sup>*Ion Beam Handbook for Materials Analysis*, edited by J. W. Mayer and E. Rimini (Academic, New York, 1977), Chap. 3.

<sup>32</sup>P. J. M. Smulders, D. O. Boerma, and M. Shaanon, *Nucl. Instrum. Methods* **B45**, 450 (1990).

<sup>33</sup>B. R. Appleton, C. Erginsoy, and W. M. Gibson, *Phys. Rev.* **161**, 330 (1967).

<sup>34</sup>J. Lindhard, K. Dan. Vidensk. Selsk. Mat. Fys. Medd. **34**, 14 (1965).

<sup>35</sup>L. C. Feldman, J. W. Mayer, and S. T. Picraux, *Materials Analysis by Ion Channeling* (Academic, New York, 1982), Chaps. 2 and 3.

<sup>36</sup>R. S. Nelson, *The Observation of Atomic Collisions in Crystalline Solids* (North-Holland, Amsterdam, 1968), Sec. 7.2 (also Wiley, New York, 1968).

<sup>37</sup>C. Erginsoy, A. Englert, and G. Vineyard, *Phys. Rev.* **133**, A595 (1964).

<sup>38</sup>J. P. Biersack and L. G. Haggmark, *Nucl. Instrum. Methods* **174**, 257 (1980); TRIM-89 copyright 1984, 1985, 1986, 1987, 1988, J. F. Ziegler, G. Cuomo, and J. P. Biersack.